



NIH PUBLIC ACCESS

Author Manuscript

ACS Appl Mater Interfaces. Author manuscript; available in PMC 2016 February 04.

Published in final edited form as:

ACS Appl Mater Interfaces. 2015 February 4; 7(4): 2891–2898. doi:10.1021/am5082556.

Detection of Viruses By Counting Single Fluorescent Genetically Biotinylated Reporter Immunophage Using a Lateral Flow Assay

Jinsu Kim¹, Meena Adhikari², Sagar Dhamane², Anna E. V. Hagström¹, Katerina Kourentzi¹, Ulrich Strych³, Richard C. Willson^{1,2,4,5,*}, and Jacinta C. Conrad^{1,*}

¹Chemical and Biomolecular Engineering, University of Houston, Houston, TX, 77204 USA

²Biology and Biochemistry, University of Houston, Houston, TX, 77204 USA

³Section of Pediatric Tropical Medicine, Baylor College of Medicine, Houston, TX 77030, USA

⁴Houston Methodist Research Institute, Houston, TX, 77030, USA

⁵Tecnológico de Monterrey, Departamento de Biotecnología e Ingeniería de Alimentos, Centro de Biotecnología FEMSA, Monterrey, Nuevo León, Mexico

Abstract

We demonstrated a lateral flow immunoassay (LFA) for detection of viruses using fluorescently-labeled M13 bacteriophage as reporters and single-reporter counting as the readout. AviTag-biotinylated M13 phage were functionalized with antibodies using avidin-biotin conjugation and fluorescently labeled with AlexaFluor 555. Individual phage bound to target viruses (here MS2 as a model) captured on an LFA membrane strip were imaged using epi-fluorescence microscopy. Using automated image processing, we counted the number of bound phage in micrographs as a function of target concentration. The resultant assay was more sensitive than enzyme-linked immunosorbent assays and traditional colloidal-gold nanoparticle LFAs for direct detection of viruses.

Keywords

Bacteriophage; diagnostics; image processing; immunoassay; lateral-flow assay; virus

Introduction

Reducing infection and mortality rates from viral pathogens, such as dengue¹ and Ebola viruses², requires rapid and early diagnosis. This need poses a special challenge in economically challenged areas with limited laboratory infrastructure where these viruses are often endemic. Early diagnosis under these conditions is aided by point-of-care (POC) diagnostics³ that are able to detect viruses at low concentrations and without involved

Corresponding Authors: willson@uh.edu; jconrad@uh.edu.

Supporting Information: Supporting Methods, including a description of the HABA assay, measurement of the degree of biotinylation, and an automated particle-counting program for magnetic beads; Supporting Results, including magnetic bead assay, evaluation of antibody attachment to Fusion 5 membranes, t-test comparison for phage assay, and replicate of phage assay. This information is available free of charge via the Internet at <http://pubs.acs.org>.

sample preparation. Traditional techniques for detecting viruses, including plaque assays and polymerase chain reaction (PCR),^{4–5} often require complex laboratory equipment and trained personnel and are therefore poorly suited for early diagnosis in these settings.

Lateral flow assays (LFAs) are a rapid, cheap, and simple option for POC diagnosis.⁶ In a typical LFA format, a biological sample containing an analyte is dispensed onto the sample pad of a porous membrane strip and transported through it by capillary action; antibodies bound to the membrane capture the analytes as they flow through the strip. Reporter particles also transported by the flow are then analyte-bridged and arrested by antibodies at the test line to produce an easily discernible line on the strip as a positive result. LFAs using gold, dyed latex, or carbon nanoparticles as reporters require minimal sample preparation and hence are routinely used in research and clinical applications.⁷ Traditional nanoparticle-based LFAs^{6–8}, however, typically cannot detect viral antigens at concentrations in clinically-useful ranges (e.g. 10^3 – 10^6 viral particles per mL for HIV-1⁹, 10^1 – 10^6 plaque forming units per mL for Ebola¹⁰, and 10^1 – 10^4 plaque forming units per mL for dengue¹¹) due to limited readout; for example, colloidal gold LFAs for Japanese encephalitis virus can detect viruses at a concentration of 2.5×10^6 pfu/mL¹² and filamentous *Escherichia coli* M13 bacteriophage (phage) at a concentration of 5×10^7 pfu/mL.¹³ By contrast, complex laboratory methods such as plaque counting and polymerase chain reaction have much lower limits of detection.^{4–5} For LFAs to be most useful as early diagnostics for viral diseases, new reporter technologies are needed with increased sensitivity and decreased limits of detection.

An intriguing alternative to the nanoparticles conventionally used as LFA reporters are viral nanoparticles, such as bacteriophage. Phage surfaces can be genetically and chemically engineered to display a wide range of functional groups, including antibodies, aptamers, lectins, peptides, proteins, and enzymes,^{14–15} enabling recognition and readout. This property allows engineered phage to serve as universal biodetection reporters in diagnostic assays,^{16–19} including enzyme-linked immunosorbent assays (ELISAs)^{20–23} and colorimetric LFAs.²⁴ In addition, phage bearing fluorescent moieties have been employed in a variety of biodetection assays that use flow cytometry^{25–29} or fluorescence microscopy^{27, 30–31} as readouts. Such fluorescently-labeled phage are of particular interest for use in LFAs, as many phage (e.g. M13, T7) are large enough to be imaged using optical microscopy as diffraction-limited objects when labeled with fluorescent dyes^{32–33} and hence can be singly counted using automated image-processing routines.³⁴ We therefore posited that the combination of coat protein engineering and fluorescence could enable a new LFA readout, in which phage reporters bound to analytes are singly counted, that may increase LFA sensitivity.

Here, we report a lateral-flow immunoassay based on enumerating individual fluorescently labeled bacteriophage reporters. We first developed a protocol to fluorescently label the p8 major coat proteins of M13, and then functionalized the p3 tail protein displaying a biotinylatable AviTag peptide with antibodies to MS2, a widely used model for viral pathogens. At each step in the protocol we confirmed that reporters were successfully modified using ELISA, 4'-hydroxyazobenzene-2-carboxylic acid (HABA) assay, and a magnetic particle counting assay. In the LFA, Fusion 5 membranes were functionalized with

test and control lines that contain antibodies to MS2 and to the M13 reporter, respectively, as shown in Figure 1. Defined numbers of MS2 phage were flowed through the LFA matrix and captured at the test line, which contained anti-MS2 antibodies. Fluorescent M13 reporters functionalized with anti-MS2 antibodies subsequently flowed through the strip were captured by the MS2 on the test line and by anti-M13 antibodies on the control line. We acquired fluorescence micrographs at the test, transition, and control lines and used automated image-processing algorithms to count the number of reporter phage at each location at the single-label level. The limit of detection (LoD) of this assay, determined from the 95% confidence intervals on the number of counted M13 reporters, is 10^2 plaque-forming units (pfu) in a 10 μ L sample deposited onto the sample pad at the end of the LFA strip, lower than that reported for colloidal-gold LFAs for viruses^{12–13} or an ELISA for MS2 virus³⁵. We anticipate that the imaging assay developed here can be integrated with inexpensive detection technologies, including paper microfluidics^{36–37} and smartphone-based fluorescence imaging,^{38–39} to enable point-of-care rapid diagnostics for viruses in resource-limited settings.

Methods

Culture and titration of MS2 viruses and M13 phage

MS2 virus (ATCC, #15597-B1) and its *E. coli* host strain (ATCC, #15597) were obtained from the American Type Culture Collection (Manassas, VA). AviTag-displaying M13 phage (AviTag-M13) were a gift from Prof. Brian Kay at the University of Illinois at Chicago. The culturing and titrating of MS2 and M13 phage were performed as described in Reference 21.

AlexaFluor 555 labeling of AviTag-M13

AviTag-M13 were modified with AlexaFluor 555 Carboxylic Acid (Succinimidyl Ester, Life Technologies #A-20009) as illustrated in Figure 2. This amine-reactive AlexaFluor 555 was conjugated to the primary amines of the p8 major coat proteins of AviTag-M13. PEG precipitation of AviTag-M13 was performed to replace the buffer in the stock solution with 0.2 M sodium bicarbonate at pH 8.3 as the optimum reaction buffer for fluorescent labeling. For PEG precipitation, 100 μ L of 10^{12} pfu/mL AviTag-M13 was mixed with 20 μ L of PEG/NaCl (20% w/v PEG 8000/2.5 M NaCl), and incubated on ice for 1 h. The PEG solution was then centrifuged at $11,000 \times g$ for 20 min at room temperature and the AviTag-M13 pellet was resuspended in 100 μ L of 0.2 M sodium bicarbonate buffer, pH 8.3. Next, 5 μ L of 10 mg/mL AlexaFluor 555 was added to the AviTag-M13 solution, and the solution was incubated overnight at 4°C on a shaker in the dark. To terminate the labeling reaction, 10 μ L of 1.5 M hydroxylamine at pH 8.5 was added to the AviTag-M13 solution and incubated for 1 h at room temperature. To remove free Alexa molecules, PEG precipitation and 7 KDa molecular weight cut-off Zeba™ spin desalting columns (Thermo Scientific #89877) were used. 100 μ L of 10^{12} /mL AviTag-FluorM13 were stored in the dark at 4°C until used.

Biotinylation of AviTag-FluorM13

AviTag-M13 phage display a peptide on the p3 tail protein which can serve as a substrate for *E. coli* biotin ligase and is inherently biotinylated at greater than 50% efficiency when grown in an *E. coli* host that contains the pBirA plasmid.⁴⁰ We completed the biotinylation

in vitro using *E. coli* biotin ligase (*birA*), according to the manufacturer's instructions (Avidity AviTag™ Technology) or using biotin ligase produced in-house. After incubation for 1 h at room temperature in the dark, excess biotinylation reagents were removed from the biotinylated FluorM13 (Biotin-FluorM13) solution via PEG precipitation and a 7K MWCO Zeba™ spin desalting column.

Neutravidin conjugation of Biotin-FluorM13

100 μL of a 10^{12} pfu/mL Biotin-FluorM13 solution was mixed with 10 μL of 0.1 mg/mL neutravidin (Thermo Fisher Scientific #31000), and the resulting solution was incubated for 1 h at room temperature in the dark. To remove excess neutravidin, the solution was dialyzed for 20 h against 1 liter of PBS using a Float-A-Lyzer 100K MWCO dialysis device (Spectra/Por #G235035) with five complete buffer changes during the dialysis.

Biotinylation of anti-MS2 antibodies

Rabbit Anti-MS2 antibodies (Tetracore, #TC-7004-002) were biotinylated using EZ-Link Sulfo-NHS-LC Biotin (Thermo Scientific #21335) following the manufacturer's protocol. In brief, 10 μL of 2.8 mg/mL anti-MS2 antibody solution was mixed with 20 μL of 0.1 mg/mL EZ-Link Sulfo-NHS-LC Biotin and 90 μL of PBS. The solution was then incubated for 30 min at room temperature. A 7K MWCO Zeba™ spin desalting column was used to remove excess biotin.

Functionalization of FluorM13 with anti-MS2 antibodies through biotin-avidin conjugation

10 μL of 0.23 mg/mL biotinylated anti-MS2 antibodies were mixed with 990 μL of 1.1×10^{11} pfu/mL neutravidin-functionalized FluorM13 in PBS and incubated for 1 h at room temperature in the dark. Excess biotinylated anti-MS2 antibody was removed using a Float-A-Lyzer 300K MWCO dialysis device with five complete buffer changes during the dialysis.

Estimation of the biotin/antibody ratio of biotinylated anti-MS2 antibodies using the HABA assay

A HABA assay (Thermo Scientific, #28005) was used to estimate the biotin/antibody ratio of biotinylated anti-MS2 antibody (additional details are given in the Supporting Information). From the difference between the absorbance of HABA/Avidin solution and that of a HABA/Avidin/Biotinylated-anti-MS2 antibody mixture measured at 500 nm, a ratio of biotin to anti-MS2 antibody of 3.1 was estimated using the analytical formula provided by the manufacturer.

Comparison of the degree of biotinylation of Biotin-FluorM13 using ELISA

The degrees of biotinylation of AviTag-FluorM13 and Biotin-FluorM13 were compared using TMB (3,3',5,5'-Tetramethylbenzidine)-ELISA. Additional details on the ELISA protocol can be found in Supporting Information.

Assessment of anti-MS2 antibody-functionalized FluorM13 using ELISA

We assessed the conjugation of rabbit anti-MS2 antibodies onto FluorM13 using ELISA. The ELISA plate was coated with 100 μL of 5 $\mu\text{g}/\text{mL}$ anti-rabbit IgG antibody (Sigma-Aldrich, #R4880) and incubated overnight at 4°C. The plate wells were washed and rinsed four times each with PBST and PBS, respectively, and blocked with 300 μL of 2% (w/v) BSA in PBS for 2 h at room temperature. 100 μL of rabbit anti-MS2 antibody-functionalized FluorM13 at concentrations of 0, 10^8 , 10^9 , and 10^{10} pfu/mL were added to the wells and incubated for 1 h at room temperature; for the negative control experiment, AviTag-FluorM13 with no antibody was added to the wells. Bound antibody-functionalized FluorM13 were allowed to react with 100 μL of HRP-conjugated anti-M13 antibody (1:5,000 dilution in 2% (w/v) BSA in PBS) for 1 h at room temperature, followed by washing and rinsing. To develop the color, 50 μL of TMB was added to the plate for 10 min, after which the reaction was terminated by addition of 50 μL of 2 N H_2SO_4 . Absorbance was measured at 450 nm in the ELISA reader.

Modification of magnetic particles with proteins

Carboxylated magnetic particles (1 μm diameter, Thermo Scientific, #4515-2105-050350) were coated with anti-M13 antibody, neutravidin, biotinylated-BSA, or anti-rabbit antibody using standard 1-Ethyl-3-(3-dimethylaminopropyl)carbodiimide-HCl-*N*-Hydroxylsuccinimide (EDC-NHS) coupling. To pre-activate magnetic particles for protein coupling, we mixed 200 μL of a 5% (w/v) solution of magnetic particles with 230 μL of 50 mg/mL NHS and 230 μL of 42 mg/mL EDC in 50 mM of MES buffer at pH 6 and diluted to 1 mL by adding 340 μL of 50 mM MES buffer. The mixture was incubated for 30 min on a rotator at room temperature. The particles were washed using a magnetic stand with 50 mM of MES buffer once and PBS twice and briefly sonicated after each wash. The magnetic particles were then resuspended in 1 mL of PBS. 100 μL of 1% EDC-NHS preactivated magnetic particles were mixed with 100 μL of one of the protein solutions (0.56 mg/mL anti-MS2 antibody, 1.5 mg/mL neutravidin, 1.5 mg/mL biotinylated-BSA, or 0.5 mg/mL anti-rabbit antibody). After 1 h incubation on a rotator at room temperature, magnetic particles were washed with PBS three times and briefly sonicated after each wash. For the first quenching step, magnetic particles were resuspended in 200 μL of 0.1 M hydroxylamine in PBS, and incubated for 1 h on a rotator at room temperature. Magnetic particles were washed with PBS three times and resuspended in 200 μL of 2% (w/v) BSA in PBS for the second quenching step. After overnight incubation, magnetic particles were washed and then resuspended with 200 μL of 0.1% (w/v) BSA in PBS and 0.005% ProClin[®]300 preservative (SUPELCO, #48126).

Magnetic particle assays for characterization of functionalized FluorM13

10 μL of a solution of protein-functionalized magnetic particles at a concentration of 1.36×10^8 particles per mL, equal to 0.01% (w/v), was mixed with 50 μL of a solution of functionalized FluorM13 at a concentration of 10^{11} pfu/mL. The mixture was incubated on a slow shaker for 1 h at room temperature in the dark and then washed six times with 0.1% (v/v) Tween 20 in PBS using a magnetic stand. The particles were then resuspended in 30 μL PBS. The particle solution was pipetted into a well chamber that was formed by placing a

silicon isolator (Grace Bio-Labs, Bend, OR; size: 4.5 mm diameter \times 1.7 mm depth) on the coverslip. A magnet was put under the coverslip for 10 sec to pull the particles down to the coverslip surface. A light microscope (Leica, DMI 3000B) equipped with a 100 \times oil immersion objective lens (NA 1.4) was used to image particles in both fluorescence and brightfield modes. To detect AlexaFluor 555 using fluorescence microscopy, samples were illuminated with a 120 W mercury lamp through a filter cube consisting of an excitation filter (BP 515–560 nm), a dichromatic mirror (580 nm), and a suppression filter (LP 590 nm). A back-thinned frame transfer CCD camera (Hamamatsu, C9100-12) was used to capture images with a 0.3 sec shutter speed. We acquired twenty pairs of brightfield and fluorescence micrographs of magnetic particles at the same focal area. Using an automated counting program (Figure S1 in Supporting Information), we counted all particles in the brightfield micrographs and the bright particles that bore bound FluorM13 in the fluorescence micrographs. We examined ~5,000 particles across each set of twenty images and calculated the fraction of bright particles by dividing the number of bright particles by the total number of particles.

Lateral flow assay

Fusion 5 strips (1 mm \times 50 mm \times 110 μ m, GE Healthcare & Life Sciences #8151-9915) were modified with 1 μ L of 0.43 mg/mL rabbit anti-M13 antibody and 1 μ L of 0.56 mg/mL rabbit anti-MS2 antibody in 50 mM acetate buffer at pH 3.6 by hand-spotting at control and test lines, respectively. MS2 virus samples were prepared with six time-serial dilutions in LFA buffer (10% BSA and 30% glycerol in PBS) at concentrations of 10^7 , 10^6 , 10^5 , 10^4 , 10^3 , 10^2 , and 0 pfu/mL. In the first step of the assay, 10 μ L of each MS2 virus sample was dispensed onto the sample pad at one end of an LFA strip. Each strip was washed with 200 μ L of washing buffer (0.1% Tween-20, 0.1% Triton X-100 in PBS). Next, 10 μ L of 10^8 pfu/mL anti-MS2 antibody-functionalized FluorM13 in LFA buffer was dispensed onto the sample pad. Each strip was washed and rinsed with 200 μ L of washing buffer and 100 μ L of PBS, respectively, to remove non-specifically bound M13 reporters. After drying in air for 1 h, the strips were immersed with pure glycerol to match the refractive index of the Fusion 5 membrane. FluorM13 reporters bound to strips were imaged using a Leica DMI 3000B fluorescence microscope equipped with a 63 \times oil immersion objective lens (NA 1.4). Micrographs were acquired at the test, transition, and control lines using a back-thinned frame transfer CCD camera (Hamamatsu, C9100-12) and analyzed using automated image-processing routines.

Results and Discussion

Characterization of FluorM13 reporter phage

To implement an imaging-based LFA format we developed novel reporter agents, fluorescent antibody-functionalized bacteriophage that were able to specifically bind to an analyte virus and were readily imaged at the single-reporter level using fluorescence microscopy. M13 bacteriophage modified to express the AviTag peptide were first fluorescently labeled with AlexaFluor 555 and subsequently conjugated with antibodies to MS2, as shown in Figure 2. Individual fluorescently-conjugated phage were readily imaged using fluorescence microscopy (Figure 3a). Subsequently, we enzymatically biotinylated the

AviTag peptide and confirmed biotinylation using a TMB-ELISA assay. The absorbance of biotin-conjugated FluorM13 on a neutravidin-coated plate was higher than that of the AviTag FluorM13 prior to conjugation, confirming that the FluorM13 phage were successfully biotinylated (Figure 3b). We prepared anti-MS2 antibodies with a ratio of 3.1 biotins per antibody and confirmed that the anti-MS2 antibodies were retained on the FluorM13 phages by ELISA (Figure 3c).

To further verify each of the FluorM13 functionalization steps, we employed a magnetic bead assay (Figure 4). We mixed magnetic particles functionalized with a variety of proteins with FluorM13 phage bearing biotin, neutravidin, or antibodies to the model virus MS2 and counted the fraction of magnetic particles that were fluorescent, signifying binding of the phage (additional details are given in the Supporting Information). For each pair of particle and phage surface chemistries, the fluorescence signal was consistent with that expected from the surface chemistries. In pairs in which specific binding was expected (e.g. between a magnetic particle functionalized with antibodies to M13 and any of the FluorM13 phage, Figure 4a, b and c) a large fraction of magnetic particles were fluorescent, confirming good binding between phage and particles. Conversely, in those cases in which specific binding was not expected (e.g. between biotin-functionalized particles and biotin-conjugated FluorM13 phage, Figure 4g) few magnetic particles were fluorescent, confirming that the phage did not bind non-specifically to the particles. We attributed the affinity of the anti-MS2 Ab FluorM13 phage for neutravidin-coated magnetic particles (Figure 4f) to the presence of excess biotins on the anti-MS2 antibody, which may bind to the neutravidin on the particles.

Automated image processing to count individual phage

To efficiently quantify the number of reporter phage bound to the LFA strip, we developed and employed an automated algorithm that locates and counts the number of the fluorescent phage in fluorescence micrographs (Figure 5; additional details on image processing methods are given in Supporting Information). The software enhanced the image contrast and increased the ratio of signal to noise, allowing phage to be counted even against a noisy or unevenly illuminated background. In addition, the image processing preserved the non-spherical shape of the FluorM13 phage, which helps to confirm their identity and allows their orientation when bound to the strip to be determined.

Imaging-LFA immunodetection of MS2 virus

To demonstrate the efficacy of our assay we chose as the analyte MS2 virus, which often serves as a model for viral pathogens. We deposited 10 μ L of a solution containing a known concentration of MS2 on a sample pad at one end of antibody-functionalized LFA strips. Capillary action transported the MS2 viruses through the strip to the test line, where anti-MS2 antibodies captured them. Anti-MS2 Ab Fluor M13 reporters subsequently transported through the strip were captured both by the MS2 viruses bound to the matrix at the test line in a sandwich and by anti-M13 antibodies at a downstream control line. The uniformly bright micrographs acquired at the control line indicated that many M13 reporters were transported through the strip (Figure 6, top row).

Individual bright spots in micrographs acquired upstream at the test line (Figure 6, bottom row) or in a non-functionalized transition region between the test and control lines (Figure 6, middle row) corresponded to individual M13 reporters bound to the strip. Resolving individual reporters required matching the refractive index of the Fusion 5 strip ($n \approx 1.5$) to the solvent, here pure glycerol. Without index matching, scattering from the strip limited our ability to resolve single phages. The low number of bound phage in the transition area at each concentration compared to the test line indicated that non-specific binding did not increase with increasing analyte concentration.

To determine the limit of detection of the imaging LFA, we quantified the number of reporters bound at the test line and in the transition region using the automated image-processing program summarized in Figure 5. The average number of bound reporters per micrograph acquired at the test line increased with increasing concentration of analyte MS2 viruses (Figure 7) but at a rate that was significantly less than linear: as the MS2 concentration was increased from 10^2 to 10^7 pfu per $10 \mu\text{L}$, the number of bound phage increased by a factor of 5. The lack of proportionality between signal and offered analyte concentration, also observed in other assays with phage reporters,^{19, 24} likely arose from steric hindrance and the great heterogeneity of the binding sites offered by the LFA matrix. The number of bound reporters in the transition area, by contrast, remained constant and independent of analyte concentration. The average number of bound reporters at the test and transition regions was different at a significance level of $p < 0.05$ for all analyte concentrations tested down to 10^2 pfu per $10 \mu\text{L}$, corresponding to a titer of 10^4 pfu/mL (Table 1 in Supporting Information). Additionally, the 95% confidence intervals for samples with nonzero MS2 concentration down to 10^2 pfu per $10 \mu\text{L}$, indicated by the notches in Figure 7, did not overlap with that of the zero MS2 concentration at the test line. Using as the criterion for the limit of detection the lack of overlap in the 95% confidence intervals of the number of bound M13 reporters, these results suggested that this assay could be used to detect as few as 10^2 pfu per $10 \mu\text{L}$. An independent replicate of the assay exhibited an identical limit of detection (Figure S4 in Supporting Information). We concluded that the limit of detection of this assay was $\sim 10^2$ pfu/strip. This LoD was approximately one-hundred-fold better than that reported for virus LFAs using gold nanoparticles as reporters^{12–13} and that reported for an ELISA³⁵ for MS2.

Conclusions

We report here a lateral flow immunoassay for viruses that employs fluorescently-labeled M13 bacteriophage as reporters. This assay relies on the fact that individual filamentous phage can be resolved and hence counted using standard fluorescence microscopy. The limit of detection for our imaging LFA was significantly better than that of conventional LFAs using gold nanoparticles^{12–13} and that of an ELISA for MS2³⁵, due in part to the resolution attained by imaging individual reporters bound to single analyte viruses.

We expect that the LoD can be lowered further by reducing nonspecific binding of the reporters in the background region and by optimizing the deposition of the test line to maximally concentrate the antibodies there. Additionally, we anticipate that tuning the chemistry and geometry of the LFA strip may further improve the LoD. An ideal strip for

this assay allows easy transport of the reporters to all antibody-functionalized sites and aids capture of the reporters; in future work we therefore plan to vary the strip material as well as the size and arrangement of the pores therein. Finally, because reporters must be readily transported throughout the strip, we surmise that the shape of the reporter phage may affect the LoD; to test this idea, we will test the efficacy of functionalized viral nanoparticles of varying morphologies as reporters in this assay.

We envision that the imaging-based LFA described here can be integrated with other advances in detection to generate a simple and inexpensive diagnostic for viruses that is suitable for point-of-care applications. Adapting our LFA into a paper microfluidics format has the potential to reduce the number of handling steps and decrease costs, and would thus be promising for use in areas with few trained medical workers⁴³. Fluorescence has already enabled multiplexed detection in a variety of modified LFAs⁴⁴ and multiplexed fluorescence imaging is easy to implement in our assay format. Similarly, combining our LFA with smartphone-based imaging methods^{39, 45}, which have already been used to image individual viruses³⁸, would generate a portable diagnostic. Moreover, recent advances in 3-D printing have demonstrated smartphone-compatible imaging systems that can magnify at 1,000x (the magnification used in this study), and cost less than a dollar for all materials⁴⁶, compatible with point-of-care diagnostics in resource-limited settings.

Supplementary Material

Refer to Web version on PubMed Central for supplementary material.

Acknowledgments

This work was funded in part by the UH Grants to Enhance and Aid Research (GEAR) program [to JCC and US], the Welch Foundation [E-1264, to RCW], NIAID/NIH [U54 AI057156, to RCW] and NSF [CBET-1133965, to RCW, and DMR-1151133, to JCC]. AEVH acknowledges postdoctoral fellowships from the Olle Engkvist Byggmästare Foundation and the Carl Trygger Foundation. The contents of this paper are solely the responsibility of the authors and do not necessarily represent the official views of the funding agencies.

References

1. Sharp TM, Gaul L, Muehlenbachs A, Hunsperger E, Bhatnagar J, Lueptow R, Santiago GA, Munoz-Jordan JL, Blau DM, Ettestad P, Bissett JD, Ledet SC, Zaki SR, Tomashek KM. Fatal Hemophagocytic Lymphohistiocytosis Associated with Locally Acquired Dengue Virus Infection - New Mexico and Texas, 2012. *Morb Mortal Wkly Rep.* 2014; 63:49–54.
2. Gire SK, Goba A, Andersen KG, Sealfon RS, Park DJ, Kanneh L, Jalloh S, Momoh M, Fullah M, Dudas G, Wohl S, Moses LM, Yozwiak NL, Winnicki S, Matranga CB, Malboeuf CM, Qu J, Gladden AD, Schaffner SF, Yang X, Jiang PP, Nekoui M, Colubri A, Coomber MR, Fonnies M, Moigboi A, Gbakie M, Kamara FK, Tucker V, Konuwa E, Saffa S, Sellu J, Jalloh AA, Kovoma A, Koninga J, Mustapha I, Kargbo K, Foday M, Yillah M, Kanneh F, Robert W, Massally JL, Chapman SB, Bochicchio J, Murphy C, Nusbaum C, Young S, Birren BW, Grant DS, Scheiffelin JS, Lander ES, Happi C, Gevaio SM, Gnirke A, Rambaut A, Garry RF, Khan SH, Sabeti PC. Genomic Surveillance Elucidates Ebola Virus Origin and Transmission During the 2014 Outbreak. *Science.* 2014; 345:1369–1372. [PubMed: 25214632]
3. Giljohann DA, Mirkin CA. Drivers of Biodiagnostic Development. *Nature.* 2009; 462:461–464. [PubMed: 19940916]

4. Uyeki TM, Prasad R, Vukotich C, Stebbins S, Rinaldo CR, Ferng YH, Morse SS, Larson EL, Aiello AE, Davis B, Monto AS. Low Sensitivity of Rapid Diagnostic Test for Influenza. *Clin Infect Dis*. 2009; 48:e89–e92. [PubMed: 19323628]
5. Izzo MM, Kirkland PD, Gu X, Lele Y, Gunn AA, House JK. Comparison of Three Diagnostic Techniques for Detection of Rotavirus and Coronavirus in Calf Faeces in Australia. *Aust Vet J*. 2012; 90:122–129. [PubMed: 22443326]
6. Posthuma-Trumpie GA, Korf J, van Amerongen A. Lateral Flow (Immuno)assay: Its Strengths, Weaknesses, Opportunities and Threats. A Literature Survey. *Anal Bioanal Chem*. 2009; 393:569–582. [PubMed: 18696055]
7. Bamrungsap S, Apiwat C, Chantima W, Dharakul T, Wiriyachaiorn N. Rapid and Sensitive Lateral Flow Immunoassay for Influenza Antigen using Fluorescently-Doped Silica Nanoparticles. *Microchim Acta*. 2014; 181:223–230.
8. Battaglioli G, Nazarian EJ, Lamson D, Musser KA, St George K. Evaluation of the RIDAQuick Norovirus Immunochromatographic Test Kit. *J Clin Virol*. 2012; 53:262–264. [PubMed: 22226980]
9. Mellors JW, Rinaldo CR, Gupta P, White RM, Todd JA, Kingsley LA. Prognosis in HIV-1 Infection Predicted by the Quantity of Virus in Plasma. *Science*. 1996; 272:1167–1170. [PubMed: 8638160]
10. Towner JS, Rollin PE, Bausch DG, Sanchez A, Crary SM, Vincent M, Lee WF, Spiropoulou CF, Ksiazek TG, Lukwiya M, Kaducu F, Downing R, Nichol ST. Rapid Diagnosis of Ebola Hemorrhagic Fever by Reverse Transcription-PCR in an Outbreak Setting and Assessment of Patient Viral Load as a Predictor of Outcome. *J Virol*. 2004; 78:4330–4341. [PubMed: 15047846]
11. de la Cruz-Hernandez SI, Flores-Aguilar H, Gonzalez-Mateos S, Lopez-Martinez I, Alpuche-Aranda C, Ludert JE, del Angel RM. Determination of Viremia and Concentration of Circulating Nonstructural Protein 1 in Patients Infected with Dengue Virus in Mexico. *Am J Trop Med Hyg*. 2013; 88:446–454. [PubMed: 23339203]
12. Li Y, Hou L, Ye J, Liu X, Dan H, Jin M, Chen H, Cao S. Development of a Convenient Immunochromatographic Strip for the Diagnosis of Infection with Japanese Encephalitis Virus in Swine. *J Virol Meth*. 2010; 168:51–56.
13. Mashayekhi F, Chiu RYT, Le AM, Chao FC, Wu BM, Kamei DT. Enhancing the Lateral-Flow Immunoassay for Viral Detection Using an Aqueous Two-Phase Micellar System. *Anal Bioanal Chem*. 2010; 398:2955–2961. [PubMed: 20865404]
14. Mateu M. Virus Engineering: Functionalization and Stabilization. *Protein Eng Des Sel*. 2011; 24:53–63. [PubMed: 20923881]
15. Yang SH, Chung WJ, McFarland S, Lee SW. Assembly of Bacteriophage into Functional Materials. *Chem Rec*. 2013; 13:43–59. [PubMed: 23280916]
16. Douglas T, Young M. Viruses: Making Friends with Old Foes. *Science*. 2006; 312:873–875. [PubMed: 16690856]
17. Zhang H, Xu Y, Huang Q, Yi C, Xiao T, Li Q. Natural Phage Nanoparticle-Mediated Real-Time Immuno-PCR for Ultrasensitive Detection of Protein Marker. *Chem Commun*. 2013; 49:3778–3780.
18. Citorik RJ, Mimeo M, Lu TK. Bacteriophage-Based Synthetic Biology for the Study of Infectious Diseases. *Curr Opin Microbiol*. 2014; 19:59–69. [PubMed: 24997401]
19. Litvinov J, Hagström AEV, Lopez Y, Adhikari M, Kourentzi K, Strych U, Monzon FA, Foster W, Cagle PT, Willson RC. Ultrasensitive Immuno-Detection Using Viral Nanoparticles with Modular Assembly Using Genetically-Directed Biotinylation. *Biotechnol Lett*. 2014; 36:1863–1868. [PubMed: 24930095]
20. Kim HJ, Ahn KC, González-Techera A, González-Sapienza GG, Gee SJ, Hammock BD. Magnetic Bead-Based Phage Anti-Immunoassay (PHAIA) for the Detection of the Urinary Biomarker 3-Phenoxybenzoic Acid to Assess Human Exposure to Pyrethroid Insecticides. *Anal Biochem*. 2009; 386:45–52. [PubMed: 19101498]
21. Kim HJ, Rossotti MA, Ahn KC, González-Sapienza GG, Gee SJ, Musker R, Hammock BD. Development of a Noncompetitive Phage Anti-Immunoassay for Brominated Diphenyl Ether 47. *Anal Biochem*. 2010; 401:38–46. [PubMed: 20152791]

22. Kim HJ, McCoy M, Gee SJ, González-Sapienza GG, Hammock BD. Noncompetitive Phage Anti-Immune-complex Real-Time Polymerase Chain Reaction for Sensitive Detection of Small Molecules. *Anal Chem.* 2011; 83:246–253. [PubMed: 21141939]
23. Brasino M, Lee JH, Cha JN. Creating Highly Amplified Enzyme-Linked Immunosorbent Assay Signals from Genetically Engineered Bacteriophage. *Anal Biochem.* 2015; 470:7–13. [PubMed: 25447463]
24. Adhikari M, Dhamane S, Hagström AEV, Garvey G, Chen WH, Kourentzi K, Strych U, Willson RC. Functionalized Viral Nanoparticles as Ultrasensitive Reporters in Lateral-Flow Assays. *Analyst.* 2013; 138:5584–5587. [PubMed: 23905160]
25. Goodridge L, Chen J, Griffiths M. Development and Characterization of a Fluorescent-Bacteriophage Assay for Detection of *Escherichia coli* O157: H7. *Appl Environ Microbiol.* 1999; 65:1397–1404. [PubMed: 10103228]
26. Goodridge L, Chen J, Griffiths M. The Use of a Fluorescent Bacteriophage Assay for Detection of *Escherichia coli* O157:H7 in Inoculated Ground Beef and Raw Milk. *Int J Food Microbiol.* 1999; 47:43–50. [PubMed: 10357272]
27. Namura M, Hijikata T, Miyanaga K, Tanji Y. Detection of *Escherichia coli* with Fluorescent Labeled Phages That Have a Broad Host Range to *E. coli* in Sewage Water. *Biotechnol Progr.* 2008; 24:481–486.
28. Carrico ZM, Farkas ME, Zhou Y, Hsiao SC, Marks JD, Chokhawala H, Clark DS, Francis MB. N-Terminal Labeling of Filamentous Phage to Create Cancer Marker Imaging Agents. *ACS Nano.* 2012; 6:6675–6680. [PubMed: 22830952]
29. Domaille DW, Lee JH, Cha JN. High density DNA Loading on the M13 Bacteriophage Provides Access to Colorimetric and Fluorescent Protein Microarray Biosensors. *Chem Commun.* 2013; 49:1759–1761.
30. Tanji Y, Furukawa C, Na SH, Hijikata T, Miyanaga K, Unno H. *Escherichia coli* Detection by GFP-Labeled Lysozyme-Inactivated T4 Bacteriophage. *J Biotechnol.* 2004; 114:11–20. [PubMed: 15464594]
31. Awais R, Fukudomi H, Miyanaga K, Unno H, Tanji Y. A Recombinant Bacteriophage-Based Assay for the Discriminative Detection of Culturable and Viable but Nonculturable *Escherichia coli* O157:H7. *Biotechnol Progr.* 2006; 22:853–859.
32. Zeng L, Skinner SO, Zong C, Sippy J, Feiss M, Golding I. Decision Making at a Subcellular Level Determines the Outcome of Bacteriophage Infection. *Cell.* 2010; 141:682–691. [PubMed: 20478257]
33. Han JH, Wang MS, Das J, Sudheendra L, Vonasek E, Nitin N, Kennedy IM. Capture and Detection of T7 Bacteriophages on a Nanostructured Interface. *ACS Appl Mater Interfaces.* 2014; 6:4758–4765. [PubMed: 24650205]
34. Adiga PS, Malladi R, Baxter W, Glaeser RM. A Binary Segmentation Approach for Boxing Ribosome Particles in Cryo EM Micrographs. *J Struct Biol.* 2004; 145:142–151. [PubMed: 15065681]
35. McBride MT, Gammon S, Pitesky M, O'Brien TW, Smith T, Aldrich J, Langlois RG, Colston B, Venkateswaran KS. Multiplexed Liquid Arrays for Simultaneous Detection of Simulants of Biological Warfare Agents. *Anal Chem.* 2003; 75:1924–1930. [PubMed: 12713052]
36. Yetisen AK, Akram MS, Lowe CR. Paper-Based Microfluidic Point-of-Care Diagnostic Devices. *Lab Chip.* 2013; 13:2210–2251. [PubMed: 23652632]
37. Hu J, Wang S, Wang L, Li F, Pingguan-Murphy B, Lu TJ, Xu F. Advances in Paper-Based Point-of-Care Diagnostics. *Biosens Bioelectron.* 2014; 54:585–597. [PubMed: 24333570]
38. Wei Q, Qi H, Luo W, Tseng D, Ki SJ, Wan Z, Göröcs Z, Bentolila LA, Wu TT, Sun R, Ozcan A. Fluorescent Imaging of Single Nanoparticles and Viruses on a Smart Phone. *ACS Nano.* 2013; 7:9147–9155. [PubMed: 24016065]
39. Vashist SK, Mudanyali O, Schneider EM, Zengerle R, Ozcan A. Cellphone-Based Devices for Bioanalytical Sciences. *Anal Bioanal Chem.* 2014; 406:3263–3277. [PubMed: 24287630]
40. Scholle MD, Kriplani U, Pabon A, Sishtla K, Glucksman MJ, Kay BK. Mapping Protease Substrates by Using a Biotinylated Phage Substrate Library. *Chembiochem.* 2006; 7:834–838. [PubMed: 16628754]

41. Malladi, R.; Ravve, I. Fast Difference Schemes for Edge Enhancing Beltrami Flow. In: Heyden, A.; Sparr, G.; Nielsen, M.; Johansen, P., editors. *Computer Vision — ECCV 2002*. Springer; Berlin Heidelberg: 2002. p. 343-357.
42. Dillencourt MB, Samet H, Tamminen M. A General-Approach to Connected-Component Labeling for Arbitrary Image Representations. *J ACM*. 1992; 39:253–280.
43. Martinez AW, Phillips ST, Whitesides GM, Carrilho E. Diagnostics for the Developing World: Microfluidic Paper-Based Analytical Devices. *Anal Chem*. 2010; 82:3–10. [PubMed: 20000334]
44. Xu Y, Liu Y, Wu Y, Xia X, Liao Y, Li Q. Fluorescent Probe-Based Lateral Flow Assay for Multiplex Nucleic Acid Detection. *Anal Chem*. 2014; 86:5611–5614. [PubMed: 24892496]
45. Ozcan A. Mobile Phones Democratize and Cultivate Next-Generation Imaging, Diagnostics and Measurement Tools. *Lab Chip*. 2014; 14:3187–3194. [PubMed: 24647550]
46. [accessed 10-13-2014] PNNL Smartphone Microscope. <http://availabletechnologies.pnnl.gov/technology.asp?id=393>

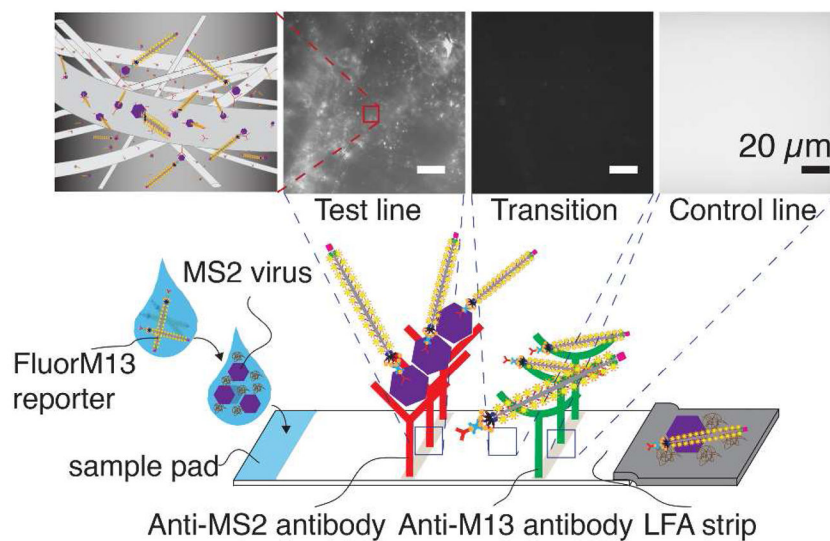


Figure 1. Imaging lateral flow assay with FluorM13 reporters

Anti-M13 and anti-MS2 antibodies were hand-spotted on Fusion 5 strips to generate test and control lines, respectively. The MS2 viruses were dispensed onto distal end of strips that were then washed in buffer. The FluorM13 reporters were spotted on the strips to sandwich MS2 viruses at the test line. Fluorescence micrographs were acquired at the test line, transition, and control line and analyzed using automated-image-processing routines to count the FluorM13 reporters.

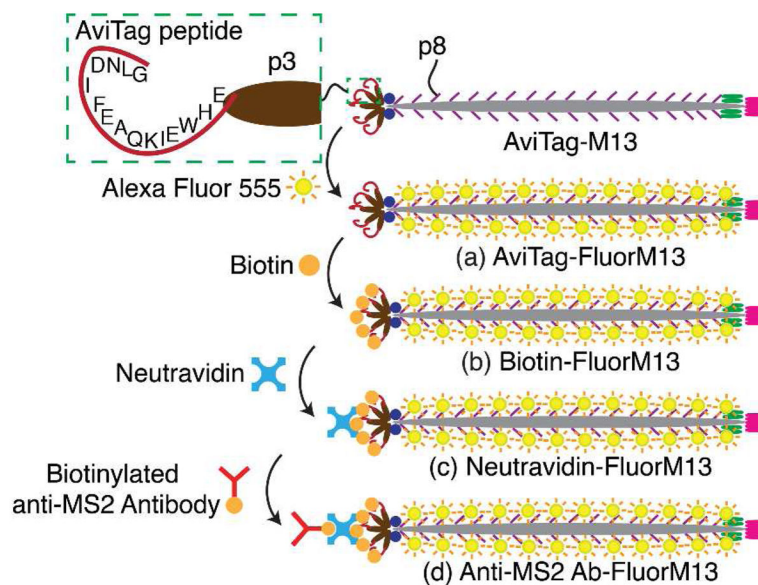


Figure 2. Modification of AviTag-M13

(a) AviTag-M13 was modified with AlexaFluor 555 on the p8 major coat proteins. (b) AviTag peptides of AviTag-FluorM13 were biotinylated on the p3 tail protein *in vitro* using biotin ligase. (c) Neutravidin was conjugated onto biotin of Biotin-FluorM13 phage. (d) Biotinylated anti-MS2 antibody was attached to Neutravidin-FluorM13 through biotin-avidin conjugation.

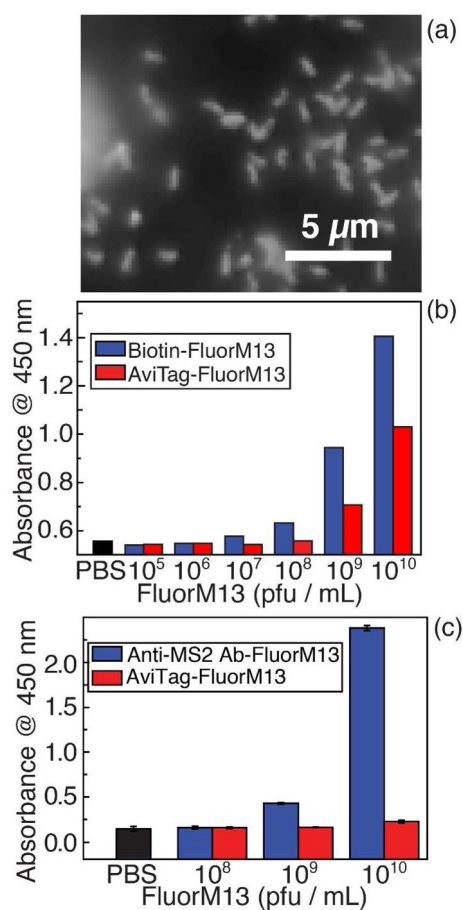


Figure 3. Characterization of modified FluorM13 reporters

(a) Fluorescence micrograph of FluorM13, demonstrating the ability to resolve individual reporter phage. (b) TMB-ELISA showing absorbance at 450 nm as a function of Biotin-FluorM13 concentration offered to bind on a streptavidin-coated plate. (c) TMB-ELISA showing absorbance at 450 nm as a function of FluorM13 concentration to confirm anti-MS2 antibody retention on FluorM13. Error bars indicate standard deviations from triplicate measurements.

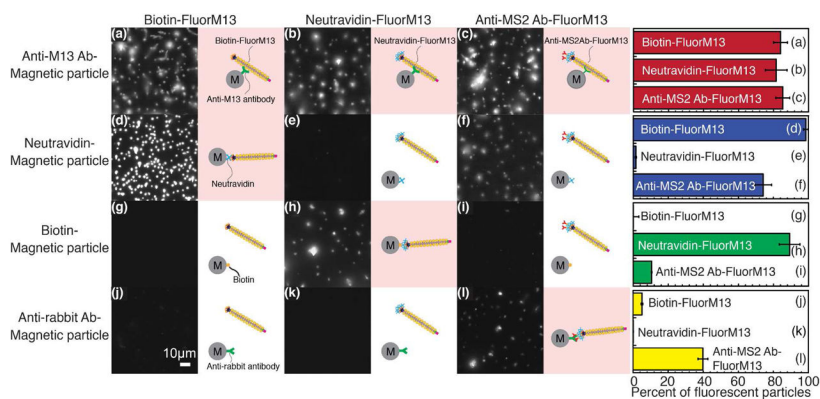


Figure 4. Characterization of modified FluorM13 reporters using magnetic particles FluorM13 functionalized with biotin, neutravidin, anti-MS2 antibody were captured by anti-M13 antibody-magnetic particles (a, b and c). Neutravidin magnetic particles showed high binding affinity with Biotin-FluorM13 (d). The affinity between neutravidin-magnetic particles and anti-MS2 Ab FluorM13 (f) was ascribed to excess biotins on the biotinylated anti-MS2 antibody based on the result of the HABA assay. The third (g, h and i) and fourth (j, k and l) rows showed that biotin-FluorM13 undergo successful neutravidin and anti-MS2 Ab conjugation, respectively. The bar graphs showed the fraction of fluorescence magnetic particles bearing bound FluorM13, corresponding to the representative micrographs. Error bars were standard deviations from twenty images analyzed for each pair of magnetic particles and modified FluorM13. All images were acquired with identical imaging conditions (camera gain = 8, camera exposure time = 0.3 sec, 100× objective lens).

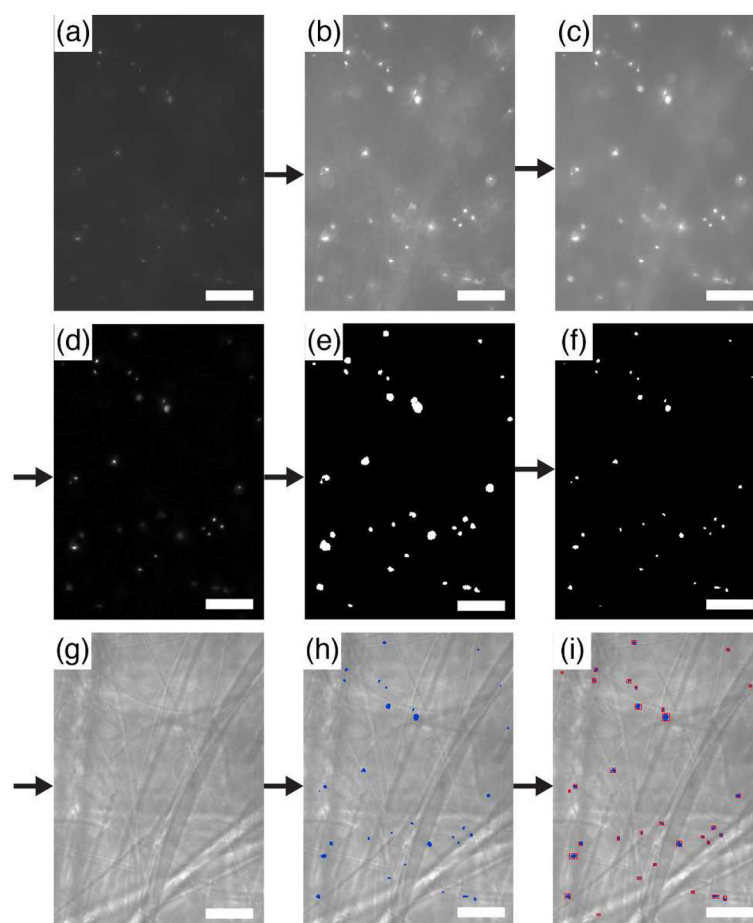


Figure 5. Automated counting of individual FluorM13 reporters

(a) A fluorescence micrograph was acquired at the LFA test line. (b) Histogram equalization³⁴ was used to enhance image contrast, allowing FluorM13 reporters to be clearly visible. (c) The Beltrami flow algorithm⁴¹ was used to reduce and smooth background noise and increase the ratio of signal to noise, while preserving the shape of the FluorM13 reporters. (d) A rank-leveling algorithm³⁴ was used to remove uneven illumination. (e, f) Global and local thresholds³⁴ were used to segment FluorM13 reporters from the background. (g) Brightfield micrograph acquired at the same focal area as in (a) of the LFA test line. (h) A connected component labeling algorithm⁴² was used to automatically count FluorM13 reporters. The segmented M13 phage reporters were overlaid onto the brightfield micrograph. (i) FluorM13 identified by the algorithm were indicated by axis-aligned bounding boxes. The scale bar for all images is 10 μm .

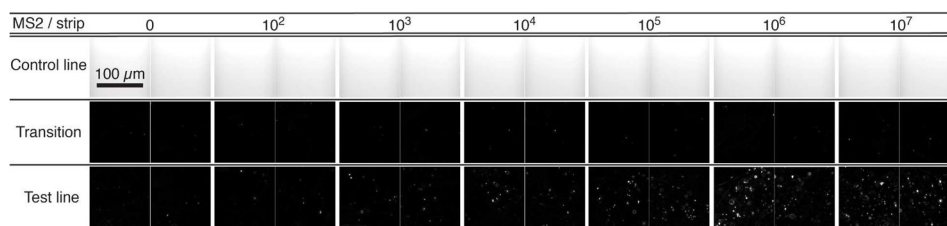


Figure 6. Representative micrographs from imaging LFAs for MS2 virus detection

For each concentration of MS2/strip, two fluorescence micrographs acquired at the control (top; saturated white), transition (middle), and test (bottom) lines are shown. Each micrograph was of dimension $130 \times 130 \text{ Jm}^2$ and the area of the antibody spotted onto Fusion 5 strips was $\sim 1 \text{ mm}^2$, so that at most sixty micrographs could be acquired from each antibody spot at a two dimensional plane. In the assay, twenty micrographs were acquired at the control, transition, and test lines of an LFA strip. We observed high fluorescence intensity at the control lines, leading to the bright white images. Although individual FluorM13 reporters cannot be distinguished at the control line, the high fluorescence intensity showed that sufficient FluorM13 reporters migrate along the length of the strip. The number of FluorM13 reporters bound at the test line increased with increasing number of MS2 per strip, and remained invariant at the transition area.

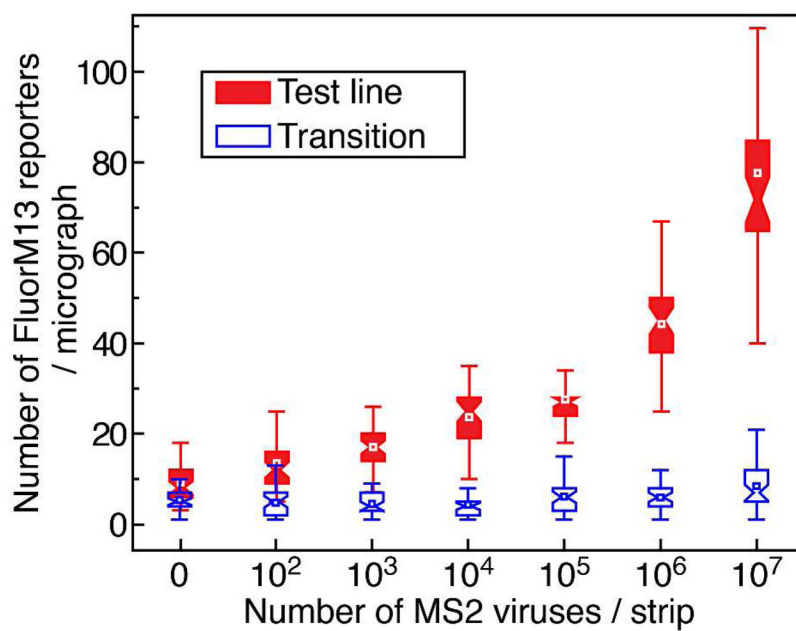


Figure 7. Limit of detection of LFA

Notch boxplot showing the number of FluorM13 reporters per micrograph as a function of number of MS2 phage per strip at LFA test line and transition region (located at 5mm further downstream from the test line). Strips were loaded with 10 JL MS2 virus solution at various concentrations. FluorM13 reporters were counted from twenty micrographs acquired for each MS2 virus concentration using an automated counting program. All test lines of LFA strips were distinguishable from the corresponding backgrounds at a statistical significance level of $p < 0.05$ using the t-test. The position of the notches indicated the 95% confidence interval; notches for images acquired at the test line for each the nonzero MS2 concentrations did not overlap with that for zero MS2 concentration.